Journal of Marine Science and Technology

Volume 30 | Issue 3 Article 1

Design and Testing of a Bearing less Piezo Jet Micro Heat Sink

Rong-Tsu Wang

Jung-Chang Wang
jcwang@mail.ntou.edu.tw

Sih-Li Chen

Recommended Citation

Wang, Rong-Tsu; Wang, Jung-Chang; and Chen, Sih-Li (2022) "Design and Testing of a Bearing less Piezo Jet Micro Heat Sink," *Journal of Marine Science and Technology*: Vol. 30: Iss. 3, Article 1.
DOI: 10.51400/2709-6998.2575
Available at: https://jmstt.ntou.edu.tw/journal/vol30/iss3/1

RESEARCH ARTICLE

Design and Testing of a Bearingless Piezo Jet Micro Heatsink

Rong-Tsu Wang [a], Jung-Chang Wang [b,*], Sih-Li Chen [c]

[a] Department of Leisure Management, Yu Da University of Science and Technology, Miaoli County 36143, Taiwan, ROC
[b] Department of Marine Engineering (DME), National Taiwan Ocean University (NTOU), Keelung 20224, Taiwan, ROC
[c] Department of Mechanical Engineering(ME), National Taiwan University(NTU), Taipei 10617, Taiwan, ROC

Abstract

The present study utilized piezoelectric ceramics (PC) as actuators to design five new piezoelectric heatsinks and preliminarily investigated the different design types and their operating conditions, such as the frequency, placement distance, thickness between piezoelectric sheets, piezoelectric sheet size, and noise produced. The results showed that when the micro heatsink bearingless piezo jet was placed too close to the heat source, the high temperature sucked back the surrounding fluids, causing the fluid chamber temperature to rise and the cooling effect to be reduced. Therefore, the heatsink should be placed between 10 and 20 mm from the heat source. With the proper distance, the heat convection coefficient was 200% greater than that of a traditional rotary fan. The cooling effect of the five heatsinks was calculated using the thermal analysis method, and the results indicated that the convection thermal resistance of the best heatsink could be reduced by about 36%, and the frequency, flow velocity, and noise were all positively correlated. When the supplied piezoelectric frequency was 300 Hz, the noise level was similar to that of a commercial rotary fan. The tested heatsinks had one of two volumes depending on the size of the piezoelectric sheet, including 3150 mm^3 or 4050 mm^3, respectively. An array of 25−32 micro heatsinks of the same size were connected in series. The power consumption of any single heatsink was 10% of that for a rotary fan. Among the five types of heatsinks, the best type had a piezoelectric sheet diameter of 41 mm, a piezoelectric thickness of 2 mm, and an opening length of 4 mm. Furthermore, the best operating conditions were found at a frequency of 300 Hz and a placement distance of 20 mm.

Keywords: Piezoelectric frequency, Actuator, Synthetic jet, Voltage, LED

1. Introduction

The compactness of the circuit modules mounted in electronic units and the rate of these circuits have been enhanced according to the advancements in IC packaging techniques and miniaturization procedures, and the operating frequency and heat generation have comparatively grown. The lifespans of these electronic components may be curtailed and their capabilities reduced if they work under excessive temperatures over a long-term period. Prescriptively, thermal engineers must depend on active or passive cooling plans for solving hotspot problems in electronics or high-temperature devices in order to lower the design cost and enhance the reliability of the system. The adoption of piezoelectric materials for heat dissipation was originally initiated in 1978 by Toda [1−4], who introduced a piezoelectric fan employing polyvinylidene fluoride resin 2 (PVF2) integrated with piezoelectric materials in the fan blades to produce a swayable cantilever beam structure. The resulting exhibit was a piezoelectric fan that could be contrasted with other small fans in conditions of their usefulness application in the heat dissipation of electronic products. Conway et al. [5] noted the cantilever beams produced markedly different wakes within the oscillation plane. They studied

Received 30 June 2021; revised 10 March 2022; accepted 21 April 2022.
Available online 12 August 2022

* Corresponding author.
E-mail address: jcwang@ntou.edu.tw (J.-C. Wang).

https://doi.org/10.514/2709-6998.2575

fans with flexible beams that were made to oscillate by tuning the alternating input voltages to the beam's resonant frequency. The results may inform the design of oscillating fans for use in thermal management applications and able to move air application in thermal applications constricted environments of position and orientation. Yoo et al. [6,7] utilized dual piezoelectric sheets to enhance the vibration behaviors of piezoelectric materials. The study investigated five patterns of dual piezoelectric sheets using distinct voltages to assess the influence of the heat exchange through gauging the amplitude of the piezoelectric materials and the wind velocity. The discoveries displayed that the harmonic vibration frequency will decrease as the length of a dual piezoelectric sheet grows, which can lessen the amount of energy wasted and the cost for mezzanines made of aluminum.

The influence of the freestream on the tip vortex is great resulting from the freestream decreasing the vortex intensity after separation from the tip or the interference of the fan with the formation of counter-rotating vortices. The peak velocity generated by a piezoelectric fan reduces at the entrance as the freestream velocity rises. The amplification in the flow velocity near the end side may be beneficent for freestreams that are slower than the peak velocity [8]. Ebrahimi et al. [9] employed experimental and numerical techniques to investigate the vortex evolution around the tips of oscillating cantilever plates with various geometries and vibrational characteristics. The vortex regimes were found to be affected by a Reynolds number (Re) based on the cantilever length. The results indicated that operating a piezoelectric fan in a propagating regime is most favorable for implementing a valid jet flow for heat transfer purposes. Ebrahimi et al. [10] showed that overcoming aerodynamic damping can account for over 50% of the total power input to a piezoelectric fan. Wu et al. [11] employed piezo electrics in the heat dissipation of electronics and adopted ANSYS software for the experiments. There were a number of differences between the experimental and simulation results. Smith and Swift [12] studied the effects of the Reynolds number and the structure of the cavity for a synthetic jet flow field, in which the faraway flow field was similar to a continuous jet flow. Under the same Re of 2000, it can create a greater jet stream than a continuous jet flow. Ko et al. [13] investigated a piezoelectric fan in motionless air utilizing the CFD and observations with an IR camera. The results showed that the temperature of the heat source could be regionally lowered by 28 °C and is very valid to cool it regionally. Kordík and Trávníček [14] found the formulation for the optimal nozzle diameter of a synthetic jet actuator utilizing a lumped element model based on the maximization of an objective function. The theoretical results were generalized into explicit relationships between the dimensionless optimal nozzle diameter and the loudspeaker parameters. A maximum overall energetic efficiency of 15% was achieved.

The scale of the turbulent kinetic energy in a piezoelectric jet is outstandingly superior compared to that in a circular jet, which can facilitate heat transfer in narrow or limited spaces [15]. The air volume flow rate of frictionless systems can be yielded through a piezoelectric fan or a dual cooling jet (DCJ) driving from a cantilever beam or a membrane resulting in disturbing the boundary layer over a hot part at a resonant frequency, revealing the enormous potential of the increase and trusty heat transfer engineering [16,17]. Jalilvand et al. [18] studied various configurations of heatsink-DCJ combinations as well as the size and shape of both heatsink and DCJ by utilizing the thermal resistance data to investigate the cooling effectiveness of the DCJ. The results revealed that more than 12 W of heat could be dissipated by the DCJ, which could easily compete with some commercialized rotary mini blowers while having a much smaller thickness. A powerful DCJ jet was revealed to generate a 24 Pa head at zero flow and 1.68 CMH at zero back pressure [19]. Shahrestani et al. [20] performed a numerical investigation on the free convection of a Newtonian fluid inside a partitioned circular enclosure at the presence of a flexible (movable) wall. The results verified that the degree of distortion (deformation) was directly dependent on the amount of force applied by the fluid. Increasing the Ra number from 10^4 to 10^7 enhanced the average Nusselt number more than five times. Moreover, increasing the Pr number from 0.71 to 200 remarkably raised the total stress applied to the plate more than 70 times.

The present study analyzed distinct design patterns involving layouts with discrepancies in the piezoelectric sheet size, spacing, and area with different types of heatsinks used in a high-power LED to determine the best heatsink to use when combining several heatsinks in series. Connecting the heatsinks in series increased the overall amount of wind and allowed for the addition or subtraction of heatsinks according to the area of the heat source to effectively control the volume of the bearingless piezo jet micro heatsink and achieve the optimal dissipation effect.

2. Research methods

Figure 1 exhibits the working principle and experimental procedure of a miniature bearingless piezoelectric radiator consisting of a circular piezoelectric sheet and made of acrylic. The frequency describes the alternating voltage periodic movement, which directly affected the operating frequency of the piezoelectric film. The operating stroke of the piezoelectric film could be divided into the expansion and compression stages, as shown in Fig. 1(a). The piezoelectric sheet was a high-voltage polarized piezoelectric ceramic sheet pasted on a metal sheet. After inputting the AC voltage, the piezoelectric effect caused mechanical deformation due to expansion and contraction. The piezoelectric sheet reciprocally coupled and oscillated with the polarity exchange frequency of the alternating current, which squeezed the air to form a jet and achieve the purpose of heat dissipation. The experimental procedure, including the structure design and the high-power LED experiment, is shown in Fig. 2(b). The research methods employed the thermal resistance network and performance measurements to determine the best design pattern for the miniature bearingless piezoelectric radiator in this study.

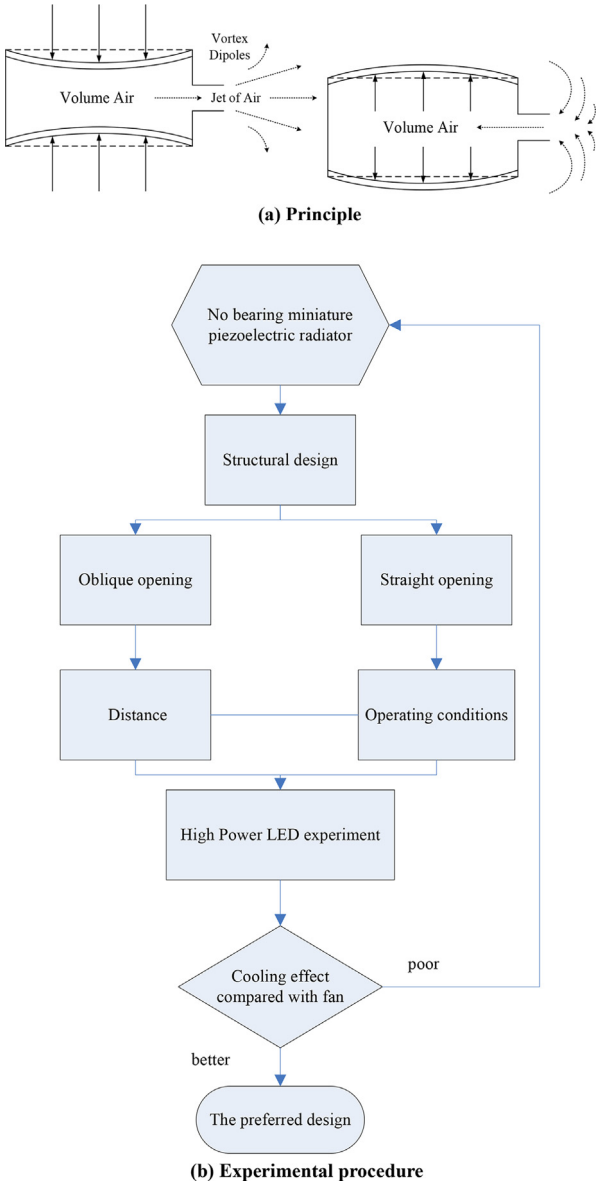

Fig. 1. Bearingless piezo jet micro heatsink.

2.1. Performance measurement

The input voltage and frequency of a piezoelectric sheet will influence the sound, deformation, and flow; therefore, the performance measurements needed to include the noise, displacement, and flow velocity parameters. The input voltage was too high to make the piezoelectric ceramic break. Therefore, the input voltage was set at 30 V, and the number of vibrations, the amount of displacement, and the flow velocity were changed according to the input voltage and frequency.

2.1.1. Noise

A handmade soundproof box was utilized for the noise experiment and a rotary fan was adopted for the subsequent experiments in the soundproof test as shown in Fig. 2. The rotary fan had performances of 21.24 CFM and 14 Pa at 2000 RPM and had the dimensions are $80 \times 80 \times 16$ mm^3. The input voltage and current were 12 V and 0.12 A, respectively. The rotary fan yielded a noise of 62.4 dB outside the box and noise of 50.7 dB inside the soundproof box. The background volume was measured to be 41.6 dB, and after correction according to the standard noise control equation, the corrected value was 50.1 dB, thus proving that the soundproof box had good soundproofing ability. The equation used for the volume correction of the background is shown as equation (1):

$$L_0 = 10log(10^{0.1L_1} - 10^{0.1L_2}) \quad (1)$$

L_0: Measured value of the intended sound source
L_1: Measured value of the total volume
L_2: Measured value of background volume

2.1.2. Displacement

Figure 3 displays the displacement measurement experiment. The space between the sensing head of the inductive displacement sensor and the

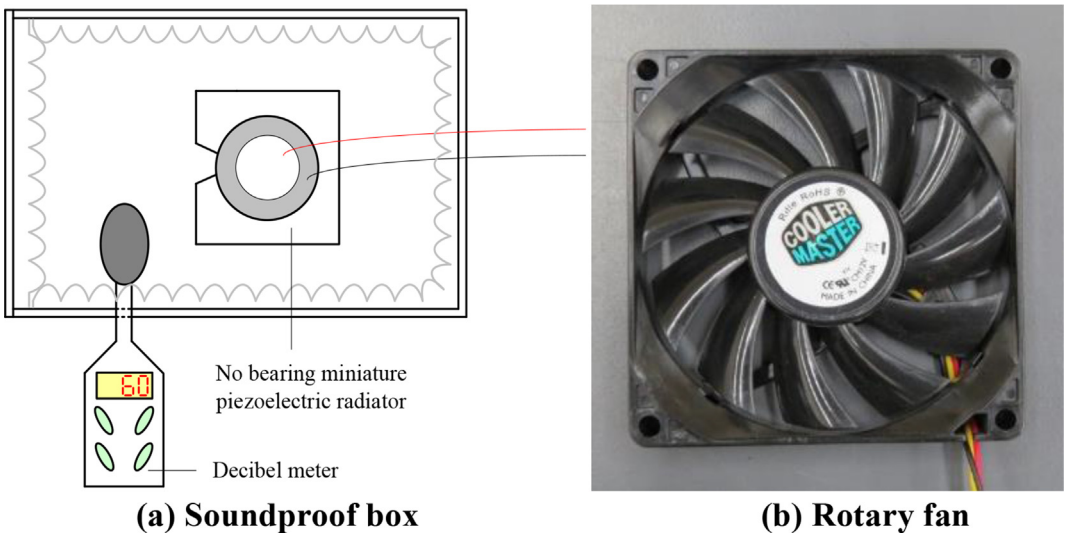

Fig. 2. Noise measurement experiment.

piezoelectric patches was 1 mm. Piezoelectric ceramics can be employed in alternating electrical energy into mechanical energy and in transferring energy to the metal foil. The displacement experiment used a clamp to tighten the heatsink and the sensing head. The high-frequency current flowing through the sensing head coil generated a high-frequency magnetic field, which intermeddled with the sensing head's degree of impedance and was alternated with the a voltage output. The displacement of the metal sheet could be computed while the voltage signal was being transmitted to the digital oscilloscope for generating waveforms.

2.1.3. Flow velocity

Figure 4 shows the flow velocity measurement experiment. The experiment was performed using a TES-1341 hot wire anemometer, which can gauge flow velocities between 0 and 30 m/s with a decision of 0.01 m/s and an error of ± 3%. The volume of air displaced by a rotary fan is inversely proportional to its placement, conventionally, and the flow velocity decreases with the increase in distance. The object of this velocity measurement experiment was to confirm the best placement between the heatsink and the heat source in order to improve the dissipation efficacy. The jet resistance raised and the dissipation efficacy may be poorer than free convection as the present heatsink is too close to the heat source. Accordingly, the position and distance are significant factors. A clamp was applied to secure the heatsink, and the space between it and the hot wire anemometer was changed in increments of 5 mm. The flow velocities were surveyed at distances of 5, 10, 15, 20, and 25 mm.

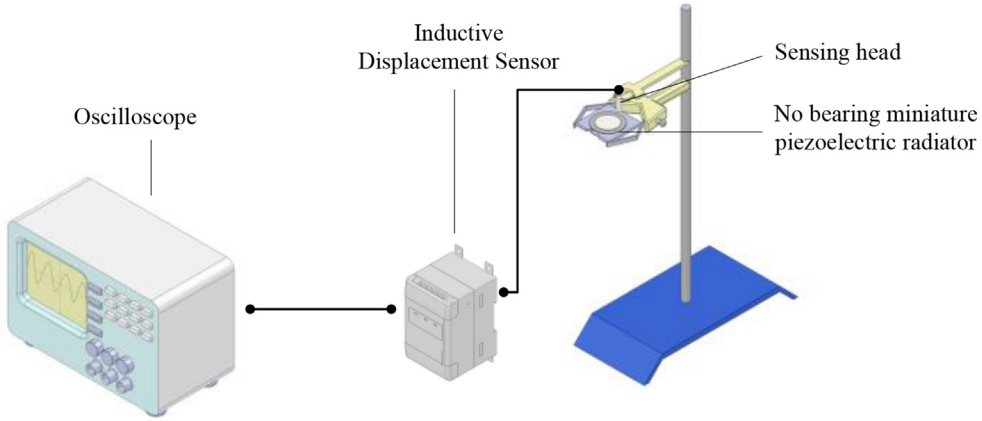

Fig. 3. Schematic diagram of displacement experiment.

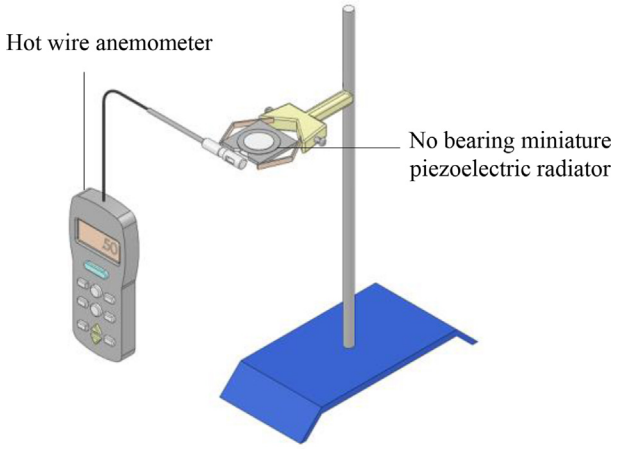

Fig. 4. Schematic diagram of velocity experiment.

2.2. Pattern design

The bearingless piezo jet micro heatsink consisted of a circular piezoelectric sheet and acrylic, which utilized a piezo-electrically driven micro heatsink. The present study investigated different design patterns involving the size, spacing, and opening area of the piezoelectric sheet. The tested radiators were divided into two types according to the design of the jet channels, as shown in Fig. 5. The first type utilized a linear jet path, as shown in Fig. 5(a), which had smooth, straight lines and a larger opening area. The second type utilized a flared jet channel, as shown in Fig. 5(b). The area of the exit was reduced and the flaring was increased, resulting in directing the airflow around the shunt and increasing the heat dissipation area. Table 1 exhibits the five different heatsinks and provides detailed specifications for comparison. Previous literature has indicated that increasing the height of the cavity will directly affect the performance of the jet strength. Therefore, the Case 5 heatsink served as the control for the Case 1 heatsink, because these two heatsinks had the same diameter and opening length, but the thickness between the piezoelectric sheets was increased from 2 mm in Case 1–3 mm in Case 5.

2.3. Thermal resistance network analysis

The high-power LED with the dimensions of 36 × 34 × 2.6 mm^3 and 3 W in the present study primarily employed the thermal resistance to evaluate the characteristics of the LED package. It can be also used to judge the dissipation capacity of a heat sink by observing the level of thermal resistance. That is, a greater thermal resistance indicates a weaker heat dissipation effect. Each temperature was measured three times under the same conditions. The definition of the thermal resistance is as the equation (2).

$$R_T = \frac{T_j - T_a}{Q} \tag{2}$$

R_T: Total thermal resistance
T_j: Temperature of the interface
T_a: Temperature of the environment
Q: Power consumption

The LED thermal resistance could be resolved for two divisions based on the present LED cooling modules. As shown in Fig. 6, the first was the thermal diffusion resistance ($R_{L,1}$) and the second was the thermal resistance of the natural convection ($R_{a,1}$). The thermal resistance of the heat diffusion ($R_{L,1}$) refers to the heat capacity that can be transferred to the substrate. Since the surface area of the substrate was greater than that of the heat source, the rate of heat diffusion was affected by the heat diffusion resistance due to the thermal conductivity of the substrate material, which could be calculated according to equation (3), which was defined as the temperature difference between the center of the LED substrate temperature ($T_{L,1}$) and the average temperature of the substrate interface ($T_{M,\ 1}$) divided by the total power (Q_{in}), shown as follows:

$$R_{L,1} = \frac{T_{L,1} - T_{M,1}}{Q_{in}} \tag{3}$$

The thermal resistance of the heat convection ($R_{a,\ 1}$) refers to the energy transmission created by the density difference between the substrate temperature and the air. A fan can also be installed to enhance the convection effect resulting in the phenomenon of forced convection, in which heat is dispersed into the air via convection. This transfer process is known as thermal convection resistance. Equation (4) defines the temperature difference between the average temperature of the substrate interface ($T_{M,\ 1}$) and the ambient temperature ($T_{a,\ 1}$) divided by the power (Q_{in}), shown as follows:

$$R_{a,1} = \frac{T_{M,1} - T_{a,1}}{Q_{in}} \tag{4}$$

To simplify in the diagram of the network analysis $R_{L,1} + R_{a,1} = R_{T,1}$ of the thermal resistance, $R_{T,1}$ was used to represent the total thermal resistance, as shown in equation (5):

$$R_{T,1} = \frac{(T_{L,1} - T_{a,1})}{Q_{in}} \tag{5}$$

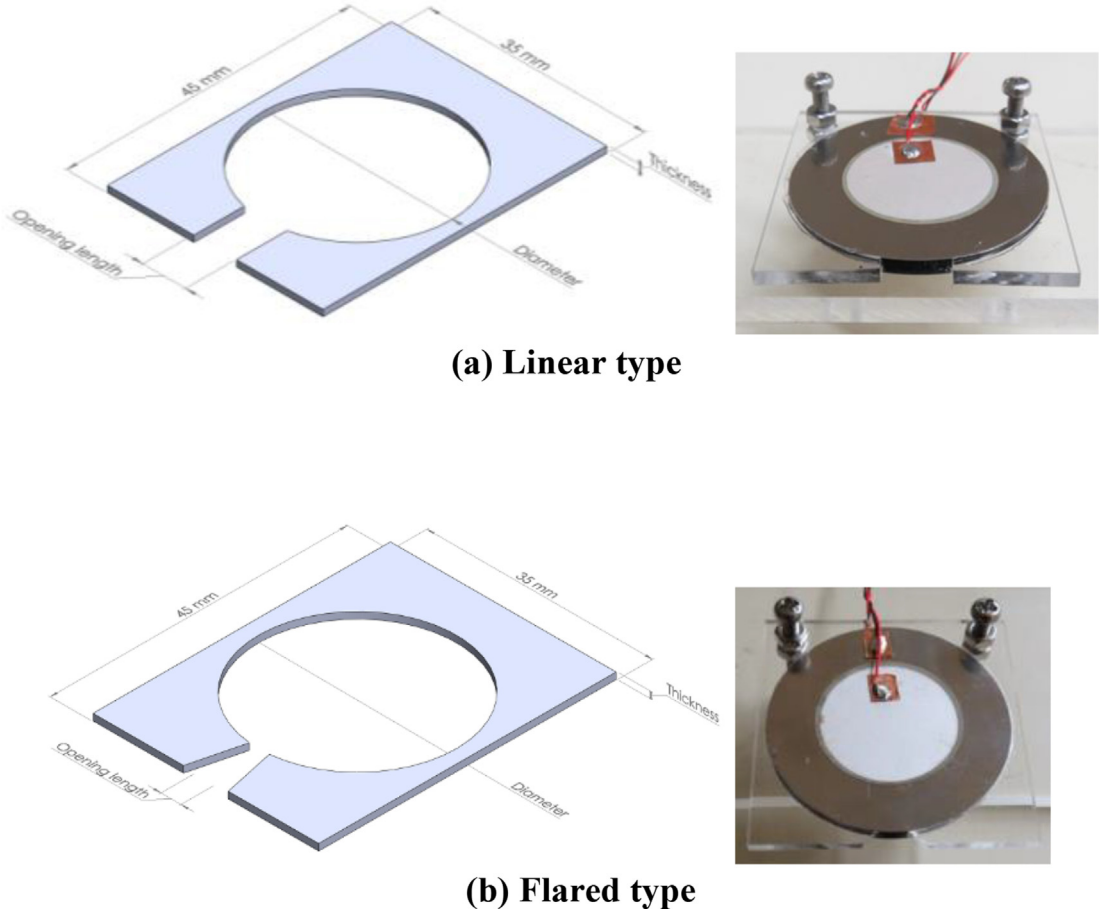

Fig. 5. Schematic diagram of jet path.

3. Results and discussion

This study focused on the characteristics of bearingless piezo jet micro heatsinks with respect to their capacity for heat dissipation when used with a high-power LED. The structural designs of the heatsinks, as well as their operating conditions and placement, were altered to investigate the impacts of such changes on the cooling effect. The best design and input conditions were selected, then, how to improve the performance of a bearingless piezo jet micro heatsink was determined.

3.1. Experiment of performance measurement

The present study examined the relevance between the frequencies and displacements of a piezoelectric metal sheet, which is a type of material that transforms electricity into sound. The noise and strength of the sounds generated depend on the voltage and the frequency supplied to the sheet. The voltage in this study was fixed at the maximum value of 30 V. The measurement range of the frequency was 50−450 Hz.

Table 1. Specifications of bearingless piezo jet micro heatsinks.

Case no.	Diameter (mm)	Cavity volume (mm^3)	Opening length (mm)	Opening area (mm^2)	Thickness (mm)
Case 1	41	2513.3	10	20	2
Case 2	41	2513.3	4	8	2
Case 3	31	1413.7	10	20	2
Case 4	31	1413.7	4	8	2
Case 5	41	3769.9	10	30	3

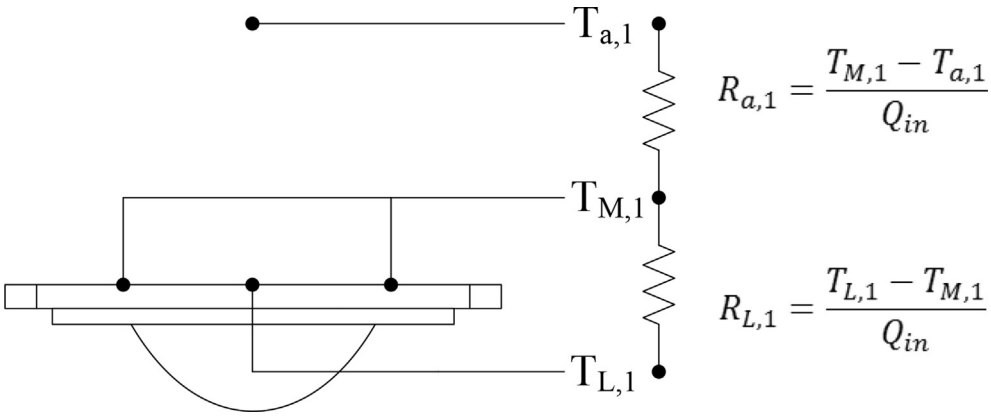

Fig. 6. LED Module network for thermal resistance.

3.1.1. Noise

Figure 7 illustrates the noise of the five bearingless piezo jet micro heatsinks, which employed a hand-made soundproof box in the present experiment. The background noise of the testing room was 41.6 dB and was 31.4 dB inside the soundproof box. Figure 7(a) shows the results for three test heatsinks—Case 1, Case 2, and Case 5—in which the diameter of the piezoelectric sheet was 41 mm. These heatsinks with piezoelectric sheets of the same size had a similar trend in terms of the growth of the noise produced. With the increase in frequency, the results of the noise strength formed line polynomials. The red dotted line demonstrates the decibel rank of 50.7 dB when the rotary fan was placed in the soundproof box. The experimental results showed that the three bearingless piezo jet micro heatsinks produced noise similar to that of the rotary fan at 300 Hz. This was 1 dB lower compared to the bearingless piezo jet micro heatsink at 300 Hz. Since the opening length was longer for the Case 1 and Case 5 heatsinks, those heatsinks had fewer places on which to fix the piezoelectric sheets compared to the Case 2 heatsink, and they caused more noise due to the free vibrations of the metal foil. At frequencies from 60 Hz to 150 Hz, however, the noise caused by the three bearingless piezo jet micro heatsinks was lower than that of the rotary fan. The thickness of the piezoelectric sheet was larger in the Case 5 heatsink. Therefore, the vibration noise produced by the heatsink was about 1–2 dB louder than that produced by the Case 1 heatsink, which is not very different. Figure 7(b) shows the results for the bearingless piezo jet micro heatsinks, in which the diameter of the piezoelectric sheet was 31 mm (i.e., the Case 3 and Case 4 heatsinks). The noise produced by the Case 3 heatsink exhibited parabolic growth, while the slope of the parabola for the Case 4 heatsink was roughly similar to a straight line. When the frequency was set at 125–225 Hz, the volume and noise for both

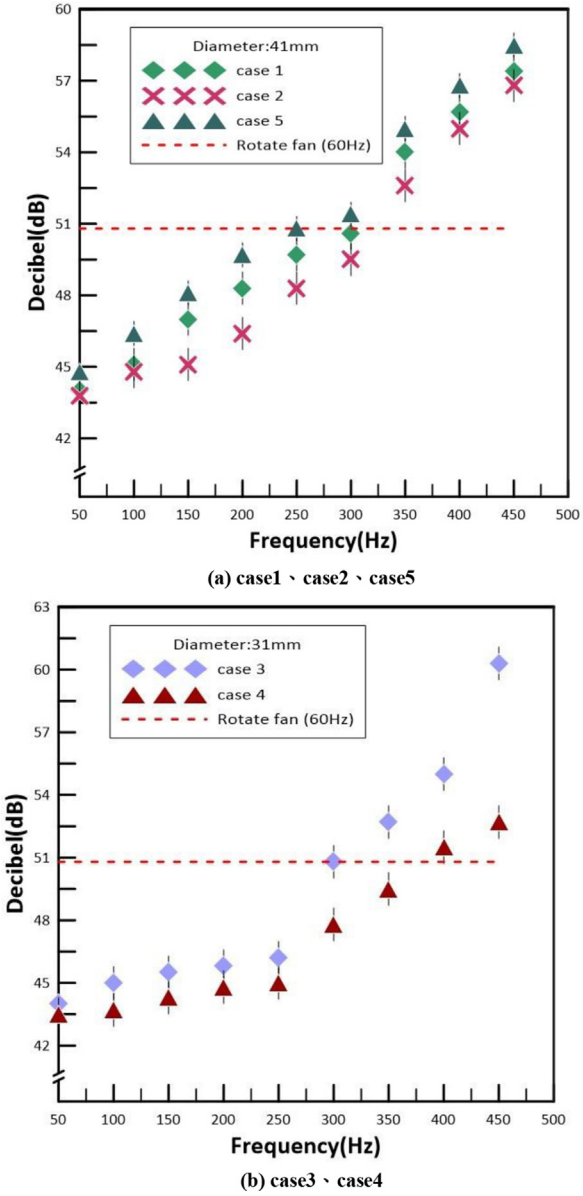

Fig. 7. The results of noise measurement.

heatsinks remained similar. Meanwhile, the Case 3 heatsink produced a higher volume than the Case 4 heatsink since it had a longer opening length. In addition, the bearingless piezo jet micro heatsinks had no wind shear effect; therefore, they could reduce the noise effectively by adopting a low operating frequency.

3.1.2. Displacement

Figure 8 shows the displacements of the five bearingless piezo jet micro heatsinks, which had similar vibration behaviors for the same types. However, the quantity of the adhesives used and the number of fixed probes were slightly different due to human error when framing the bearingless piezo jet micro heatsinks. Figure 8(a) reveals the displacement results for the test heatsinks in which the diameter of the piezoelectric sheet was 41 mm. The amount of displacement exhibited a stair-step pattern increasing every 50−100 Hz. The displacement divided by the frequency was between about 0.1 and 0.2. Figure 8(b) exhibits the displacement results for the test heatsinks in which the diameter of the piezoelectric sheet was 31 mm. When the frequency was below 280 Hz, there were no significant changes in the amount of displacement. The amount of displacement increased dramatically, however, when the frequency range was 290−300 Hz. The ratio of the displacement and the frequency was between 0.1 and 0.2. The two different types of piezoelectric sheets (31 mm and 41 mm) exhibited completely different vibration behaviors in the same measurement range, yet for both types, the ratio of the displacement and the frequency was between 0.1 and 0.2. The vibration was related to the type of piezoelectric sheet.

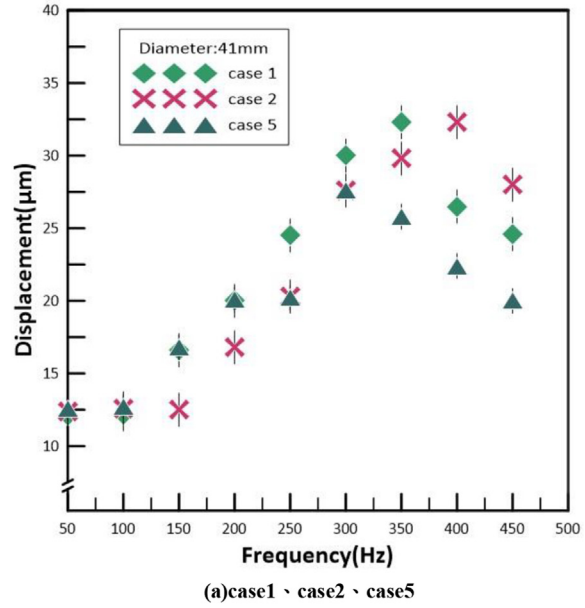

(a)case1、case2、case5

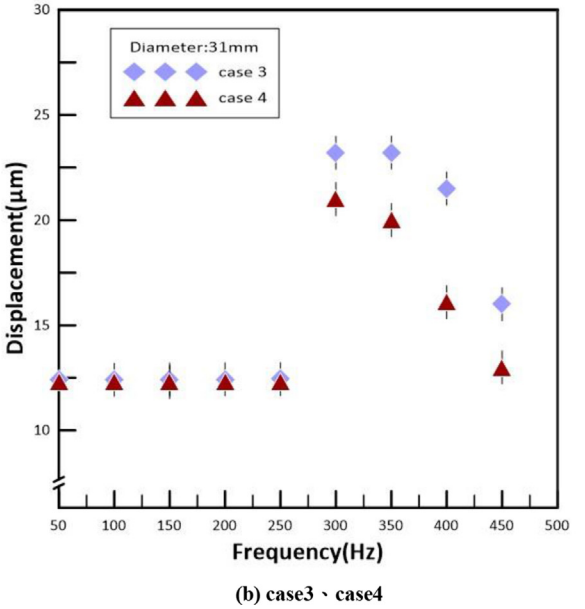

(b) case3、case4

Fig. 8. The results of displacement measurement.

3.1.3. Flow velocity

Figure 9 reveals the flow velocity of the heatsinks at different distances from the hot-wire anemometer. Since the flow velocities of the rotary fan and the piezoelectric fan were low, if the distance from the heat source was too great, the air jet would be unable to exchange heat with the heat source, and the forced convection would not function properly. In this section, the flow velocity was used to determine the cooling effect and the size of the wind velocity perturbation was regarded as an indicator of the turbulence strength. The results showed that the flow velocity and the placement of the rotary fan and heatsinks were inversely proportioned. In Case 3, the flow velocities measured at 15 mm and 20 mm were larger than at 10 mm. This was because the flow velocity was weak in Case 3 and generated a pair of vortexes at 15−20 mm to disturb the ambient air. Therefore, the flow velocity was higher. When placed at 25 mm, it was not affected. In Case 4, a larger flow velocity was generated at 20 mm, while at 25 mm it was not affected. The bearingless piezo jet micro heatsinks were unstable at low frequencies. The interval time between expansion and compression was longer so that it should be no outward expansion flow field, but only the inward airflow was into the cavity. The generation of a

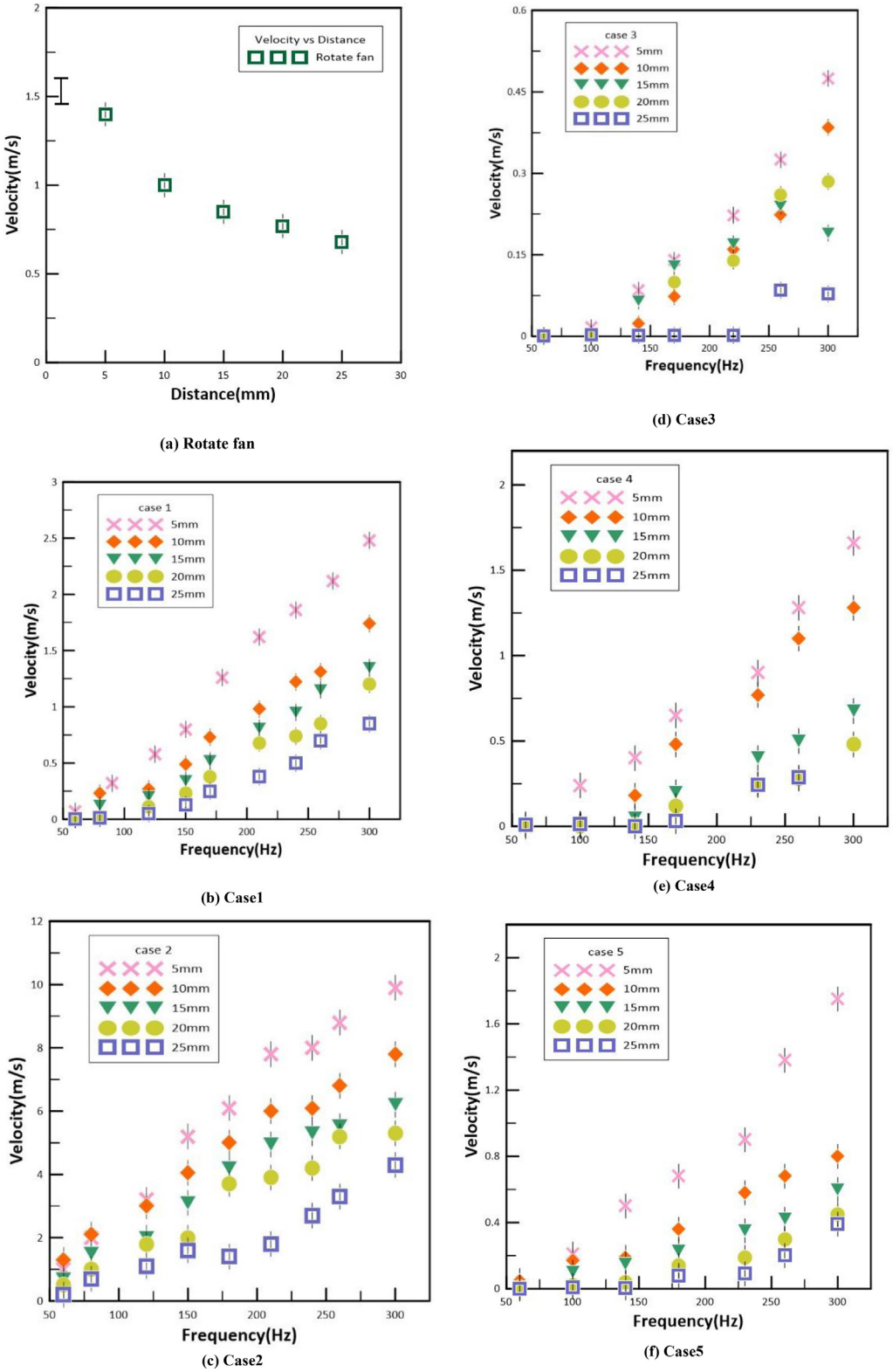

Fig. 9. Flow velocity and placement diagrams of each heatsink under different frequencies.

higher flow velocity during compression caused unstable flow velocities; therefore, the accuracy was lower. When the frequencies were above 150 Hz, the time interval was shortened. The velocity was then regarded as a continuous outward airflow, and the flow velocities were stabilized.

3.2. LED thermal performance experiment

The heatsinks employed in the present test were tested under the same operating conditions and the original 3 W LED heat source design. The ambient temperature, input voltage, and frequency were respectively 25.3 °C, 30 V, and 300 Hz. The heatsinks were placed at distances of 5 mm, 10 mm, 15 mm, 20 mm, and 25 mm to investigate the different cooling influenced by perceiving the changes in thermal resistance. The temperature of the LED module was stable after 30 min; therefore, it was recorded every 40 min. However, the power provided to the LED was not fully transformed to light. At present, the light efficiency of white LEDs is approximately 30% of the power consumed, while the other 70% is transformed to heat. Figure 10(a) compares the distances and the total thermal resistance. Among the five designs, Case 2 had the best cooling effect when placed at 20 mm. The LED module temperature was reduced to 36.4 °C, which was lower than the natural convection at 1 W. Therefore, it could continuously increase the power of the LED lights to provide better illumination capability. The worst cooling effects were achieved when placing the heatsink at 5 mm in Case 4 and at 25 mm in Case 3. From the present findings, it could be seen that although the bearingless piezo jet micro heatsink consisted of small pieces of piezoelectric sheets and had a flared jet path and a smaller thickness, its cooling effect was not ideal. This was mainly because the measured amplitude of displacement in the vibration experiment was small. The flow rate of the air that could be forced into the cavity was low and the jet strength was weak, resulting in no significant improvement in convection. When the heatsink was placed at 5 mm in Case 5, it lowered the temperature of the LED module to 26.3 °C, while Case 1 reduced the temperature to 27.1 °C. This demonstrated that the cooling performance of the heatsink worsened when increasing the distance between the piezoelectric sheets.

Figure 10(b) contrasts the distances and heat transfer coefficients. The heat transfer coefficient for Case 1 was 129 W/m^{2}K when placed at 5 mm and was reduced to 81.7 W/m^{2}K when the distance increased to 25 mm. The heat transfer coefficient for Case 2 was 132.9 W/m^{2}K when placed at 5 mm. In addition, it can upgrade to three times if placed at 20 mm. The heat transfer coefficients for Case 3 and Case 4 were about 48 and 98 W/m^{2}K, respectively. The enhanced convection efficiency was not large compared to the other bearingless piezo jet micro heatsinks, yet they could still be applied to low-wattage heat sources. Case 5 enhanced its convection efficiency by 157%−288% compared to natural convection. From the experimental results and previous analysis, it was recognized that Case 1, Case 3, and Case 5 could be applied to the heat source at a short distance. As they had a larger opening length and area, they could draw in a wider range of the air jet around with a larger air volume but a lower flow velocity. If they were placed too far from the LED heat source, they would not achieve the cooling effect. Among the five locations, the heatsink placed at 5 mm had the best cooling performance. Case 2 and Case 4 had the best heat dissipation effect at 20 mm. Case 2 and Case 4 also had a higher flow velocity, as the increased distance

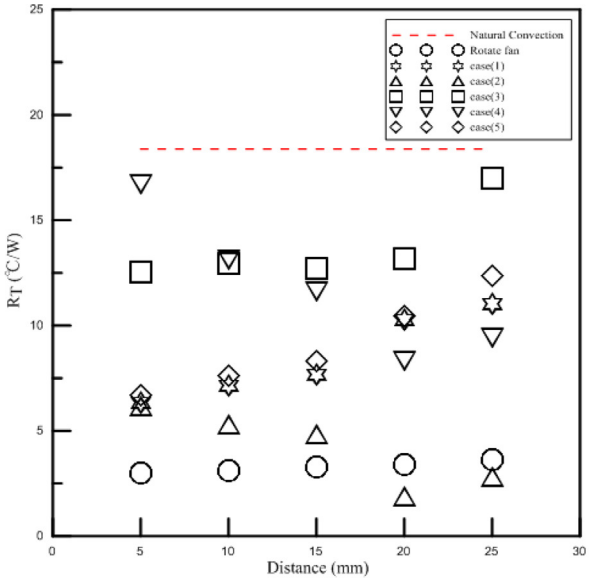

(a) Position vs total thermal resistance

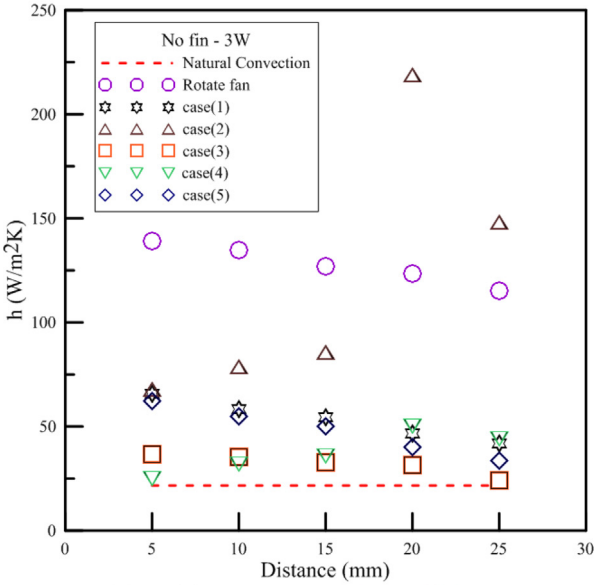

(b) Position vs heat transfer coefficient

Fig. 10. 3 W LED experimental data.

was conducive to sucking in the surrounding fluid and preventing the hot air from being sucked back again. However, the strength of the airflow was limited. The intensity of the airflow was reduced and was not advantageous to heat dissipation when the distance was expanded to 25 mm.

4. Conclusion

The present study designed a new type of piezoelectric fan and investigated the input conditions. Five bearingless piezo jet micro heatsinks were fabricated using a variety of parameters, including the piezoelectric sheet spacing, the size, and the opening area, in order to establish performance test methods and conduct cooling experiments on the heat dissipation of high-power LEDs. The results showed that the preferred design and operating conditions could fully make use of heatsinks and provide a better cooling effect than traditional rotary fans. The power consumption comparison results revealed that the power needed for the bearingless piezo jet micro heatsink to reduce the temperature to 1 °C was only 10%−25% of that for a rotary fan, and the bearingless piezo jet micro heatsink had lower costs. The area of the bearingless piezo jet micro heatsink was only 4% of current commercial rotary fans. In other words, about 25 bearingless piezo jet micro heatsinks could be connected in series while taking up no additional space, representing a completely new method of heat dispersion.

Declaration of competing interest

There is no conflict of interest.

References

[1] Toda M. Theory of air flow generation by a resonant type PVF2 bimorph cantilever vibrator. Ferroelectrics 1978;22(1):911−8.
[2] Toda M. High field dielectric loss of PVF2 and the electromechanical conversion efficiency of a PVF2 fan. Ferroelectrics 1978;22(1):919−23.
[3] Toda Minoru. Elastic properties of piezoelectric PVF2. J Appl Phys 1980;51(9):4673−7.
[4] Toda M, Osaka S. Vibrational fan using the piezoelectric polymer PVF 2. Proc IEEE 1979;67(8):1171−3.
[5] Conway C, Jeffers N, Agarwal A, Punch J. Influence of thickness on the flow field generated by an oscillating cantilever beam. Exp Fluid 2020;61(7):1−19.
[6] Yoo Ju Hyun, Hong Jae Il, Cao Wenwn. Piezoelectric ceramic bimorph coupled to thin metal plate as cooling fan for electronic devices. Sensor Actuator Phys 2000;79(1):8−12.
[7] Yoo Ju Hyun, Hong Jae Il, Chang Yub Park. Characteristics of piezoelectric fans using PZT ceramics. Proceedings of 5th International Conference on Properties and Applications of Dielectric Materials, vol. 2. IEEE; 1997.
[8] Park SH, Oh MH, Kim YH, Choi M. Effects of freestream on piezoelectric fan performance. J Fluid Struct 2019;87:302−18.
[9] Ebrahimi ND, Eldredge JD, Ju YS. Wake vortex regimes of a pitching cantilever plate in quiescent air and their correlation with mean flow generation. J Fluid Struct 2019;84:408−20.
[10] Ebrahimi ND, Wang Y, Ju YS. Sensors and actuators A: physical mechanisms of power dissipation in piezoelectric fans and their correlation with convective heat transfer performance. Sens Actuators A Phys 2018;272:242−52.
[11] Wu T, Ro PI, Kingon AI, Mulling JF. Piezoelectric resonating structures for microelectronic cooling. Smart Mater Struct 2003;12(2):181.
[12] Smith Barton L, Swift GW. A comparison between synthetic jets and continuous jets. Exp Fluid 2003;34(4):467−72.
[13] Ko J, Oh MH, Choi M. Effects of piezoelectric fan on cooling flat plate in quiescent air. Eur J Mech B Fluid 2021;88:199−207.
[14] Kordík J, Trávníček Z. Optimal diameter of nozzles of synthetic jet actuators based on electrodynamic transducers. Exp Therm Fluid Sci 2017;86:281−94.
[15] Zhou W, Yuan L, Wen X, Liu Y, Peng D. Enhanced impingement cooling of a circular jet using a piezoelectric fan. Appl Therm Eng 2019;160:114067.
[16] Strohmeyr S, Gundelsweiler B, Schinkoethe W, Baazouzi S. Cooling of linear direct drives in precision engineering with piezo fans. IKMT 2019-Innovative small Drives and Micro-Motor Systems, vol. 12. ETG/GMM-Symposium. VDE; 2019.
[17] Liu TJC, Chen YS, Ho HY, Liu JT. Vibration and cooling performances of piezoelectric cooling fan: numerical and experimental investigations. MATEC Web of Conferences, vol. 306. EDP Sciences; 2020.
[18] Jalilvand A, Mochizuki M, Saito Y, Kawahara Y, Singh R, Wuttijumnong V. Cooling performance evaluation of synthetic jet based thermal solution module. J Therm Sci Eng Appl 2015;7(3):031010.
[19] De Bock HP, Chamarthy P, Jackson JL, Whalen B. May). Investigation and application of an advanced dual piezoelectric cooling jet to a typical electronics cooling configuration. In: 13th InterSociety Conference on Thermal and Thermomechanical Phenomena in Electronic Systems. IEEE; 2012. p. 1387−94.
[20] Shahrestani AB, Alshuraiaan B, Izadi M. Combined natural convection-FSI inside a circular enclosure divided by a movable barrier. Int Commun Heat Mass Tran 2021;126:105426.